ACS APPLIED MATERIALS & INTERFACES

Research Article

www.acsami.org

Bacteria-Affinity 3D Macroporous Graphene/MWCNTs/Fe_3O_4 Foams for High-Performance Microbial Fuel Cells

Rong-Bin Song,[†] Cui-E Zhao,[‡] Li-Ping Jiang,[†] Essam Sayed Abdel-Halim,[§] Jian-Rong Zhang,*[,†,∥] and Jun-Jie Zhu*[,†]

[†]State Key Laboratory of Analytical Chemistry for Life Science and Collaborative Innovation Center of Chemistry for Life Sciences, School of Chemistry and Chemical Engineering, Nanjing University, Nanjing 210093, P. R. China

[‡]Key Laboratory for Organic Electronics and Information Displays and Institute of Advanced Materials, Nanjing University of Posts & Telecommunications, Nanjing 210023, P. R. China

[§]Chemistry Department, College of Science, King Saud University, Riyadh 11451, P. O. Box2455, Kingdom of Saudi Arabia

[∥]School of Chemistry and Life Science, Nanjing University Jinling College, Nanjing 210089, P. R. China

Supporting Information

ABSTRACT: Promoting the performance of microbial fuel cells (MFCs) relies heavily on the structure design and composition tailoring of electrode materials. In this work, three-dimensional (3D) macroporous graphene foams incorporated with intercalated spacer of multiwalled carbon nanotubes (MWCNTs) and bacterial anchor of Fe_3O_4 nanospheres (named as G/MWCNTs/Fe_3O_4 foams) were first synthesized and used as anodes for *Shewanella*-inoculated microbial fuel cells (MFCs). Thanks to the macroporous structure of 3D graphene foams, the expanded electrode surface by MWCNTs spacing, as well as the high affinity of Fe_3O_4 nanospheres toward *Shewanella oneidensis* MR-1, the anode exhibited high bacterial loading capability. In addition to spacing graphene nanosheets for accommodating bacterial cells, MWCNTs paved a smoother way for electron transport in the electrode substrate of MFCs. Meanwhile, the embedded bioaffinity Fe_3O_4 nanospheres capable of preserving the bacterial metabolic activity provided guarantee for the long-term durability of the MFCs. With these merits, the constructed MFC possessed significantly higher power output and stronger stability than that with conventional graphite rod anode.

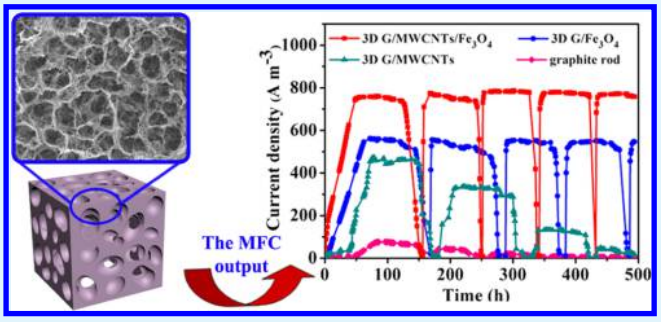

KEYWORDS: *microbial fuel cells, bioaffinity, electrochemistry, graphene foams, multiwalled carbon nanotubes*

INTRODUCTION

As a classical and widely studied example of bioelectrochemical systems (BESs), microbial fuel cells (MFCs) can fulfill the double task of wastewater treatment and electricity generation, having attracted much attention in recent years.[1−4] In MFCs, electroactive bacteria are utilized as electrocatalysts to oxidize organic molecules, directly converting chemical energy into electrical energy.[5−9] However, the low power density and poor long-term stability extremely hinder their practical application. Among numerous factors,[10−12] the anode material undertakes the function of providing area for bacterial attachment and extracellular electron transfer (EET), highly influencing the overall performance of MFCs. Therefore, extensive studies have been dedicated to developing novel anode materials for overcoming the aforementioned drawbacks.

Generally, commercially available graphite/carbon-based anodes[13−16] (e.g., graphite rod and carbon paper) are adopted as the anodic matrix in most MFCs. However, these materials inherently suffer from low EET efficiency and poor bacterial adhesion. Moreover, bacterial attachment and electron transfer only occur on the outer surface of materials, while the interior space of these electrodes remains unexploited, owing to the inner pore plugging caused by rapid bacterial growth. In view of this, many endeavors have been made to pursue three-dimensional (3D) materials for configuring high-performance MFC.[17−24] Among them, 3D graphene emerges as an attractive candidate, due to its outstanding electrical conductivity, large pore size, and high specific surface area.[25−27] However, during fabrication and drying process, 3D graphene irreversibly aggregates with $\pi-\pi$ stacking between graphene sheets (GS),[28] dramatically reducing the accessible surface area for bacterial adhesion. To solve this problem, one feasible solution is to incorporate multiwalled carbon nanotubes (MWCNTs), which have been demonstrated to be effective in preventing GS from restacking and accelerating electron transfer.[29,30]

Aside from the structure optimization of electrode materials for maximized active surface area, regulating electrode composition to improve the bacteria-electrode interactions is

Received: March 21, 2016
Accepted: June 7, 2016
Published: June 7, 2016

DOI: 10.1021/acsami.6b03425
ACS Appl. Mater. Interfaces 2016, 8, 16170−16177

Scheme 1. Fabrication of the 3D Macroporous G/MWCNTs/Fe_3O_4 Foams and Their Use as MFC Anode Materials

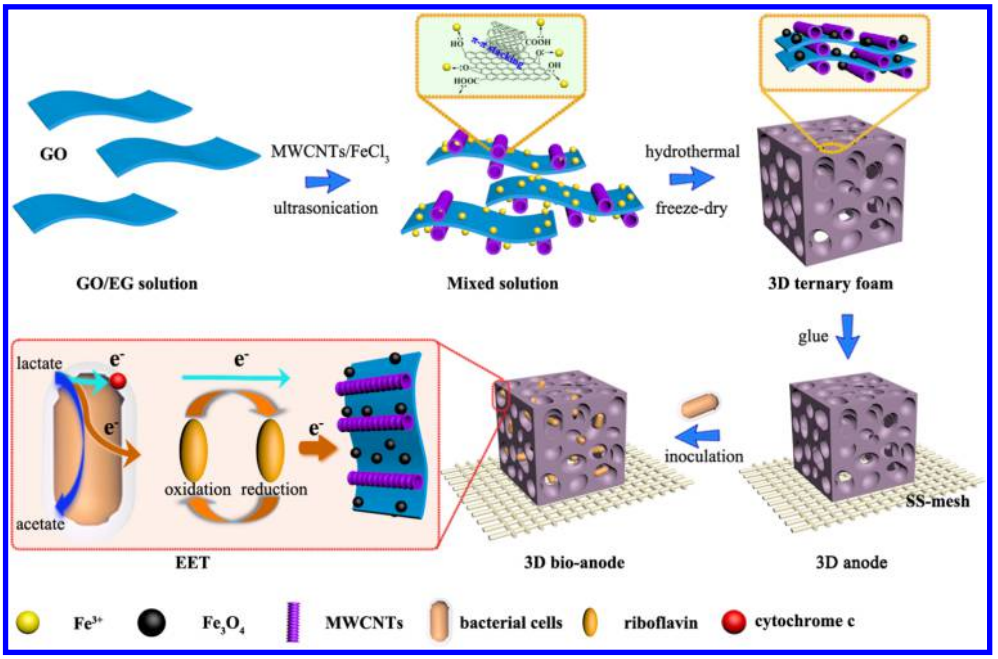

another effective route for upgrading the MFC overall performance.[31] The genus *Shewanella*, which consists of dissimilatory iron-reducing bacteria (DIRB) often used as model bacteria in MFCs due to its excellent electrogenic capacity, has the ability to recognize the surface of Fe (III) oxides and initiate EET in its metabolism.[32,33] The c-type cytochromes on outer-membrane redox proteins (OM c-cyts) mediate EET from bacterial cells to Fe (III) oxides, which act as a "molecular wire" and play an important role in the electron transfer process.[34−36] Inspired by this mechanism, we deduce that Fe (III) species have the likelihood to favorably attract bacteria and accelerate bacteria-electrode electron transport, thus contributive to elevating the MFC properties at the level of composition modulation other than morphology tailoring.

In this study, adopting MWCNTs as intercalated spacer and Fe_3O_4 nanospheres as bioaffinity anchor, we devise a novel interconnected 3D macroporous framework of graphene sheets incorporated with Fe_3O_4 nanospheres and MWCNTs (3D G/MWCNTs/Fe_3O_4 foams) via one-pot solvothermal process and freeze-dry method (Scheme 1). The resultant 3D G/MWCNTs/Fe_3O_4 foams were employed as an anode for MFCs, displaying much higher power density and better durability compared with a commercial graphite rod anode. The improved performance of MFCs with 3D G/MWCNTs/Fe_3O_4 anode could be attributed to its macropores structure, good conductivity, high affinity for the attachment of *Shewanella*, and efficient EET between microbial biofilm and anode.

EXPERIMENTAL SECTION

Chemicals and Materials. Graphite (ks-10, 99.95%) was purchased from Sigma-Aldrich. Iron(III) chloride hexahydrate ($FeCl_3·6H_2O$), sodium acetate (NaAc), and ethylene glycol (EG) were obtained from Sinopharm Chemical Reagent Co., Ltd. BCA Multiwalled carbon nanotubes were bought from Nanoport Co., Ltd. (Shenzhen, China). All the other reagents were of analytical grade and used as received. Deionized water (resistance over 18 MΩ cm at 25 °C) used in all experiments was prepared by an ultrapure water system.

3D G/MWCNTs/Fe_3O_4 Foams Preparation. GO was synthesized from natural graphite powder (ks-10, 99.95%) according to a modified Hummer's method.[37,38] 3D G/MWCNTs/Fe_3O_4 foams were fabricated by hydrothermal and cryogenic methodologies. In a typical experiment, 0.06 g of MWCNTs and 0.1 g of $FeCl_3·6H_2O$ were added into 10 mL of GO/EG (3 mg mL^{-1}) solution; after ultrasonication for 2 h in an ice bath, NaAc (0.38 g) was added to the solution, followed by vigorous stirring for 15 min to obtain stable mixed suspensions. Two milliliters of the suspensions were transferred to a vial, and then the vial was sealed in a Teflon-lined stainless steel autoclave and maintained at 250 °C for 36 h. During the hydrothermal process, along with the coupling of GO with MWCNTs, the reduction of Fe^{3+} cations to Fe_3O_4 nanospheres occurred in the presence of ethylene glycol (EG) as a reducing agent and sodium acetate as an alkali source. After it cooled, the as-prepared hybrid architecture was first dialyzed with ultrapure water (the ultrapure water was changed every 12 h) for 72 h, followed by freeze-drying to obtain 3D macroporous G/MWCNT/Fe_3O_4 hybrid foams. The mass ratio in this hybrid foam is G/MWCNTs/Fe_3O_4 = 1:2:1. To prepare 3D G/Fe_3O_4 foams and 3D G/MWCNTs foams for comparison, the same conditions and procedures were employed in the absence of MWCNTs and $FeCl_3·6H_2O$, respectively.

Electrodes Preparation. For 3D electrodes preparation, two monolithic foams (13 mm diameter, 2.5 mm height) were glued to both sides of a stainless-steel (SS, 60 × 60 mesh, type SUS304, Xinsilu Metal Product Co. Ltd., Shanghai, China) mesh.[39] The glue was conductive carbon paint (Structure Probe, Inc., SPI Supplies, USA). The SS mesh (15 mm × 20 mm) was placed in acetone for 3 h before using. The total volume of 3D electrodes was 1.3 cm^3. To keep the volume of graphite rod electrodes was the same as that of the prepared 3D electrodes, commercial available graphite rods (10 mm diameter, 10 cm height) were cut into slices (10 mm diameter, 4 mm height), which were directly glued to both sides of a SS. Prior to be glued, the slices were sterilized in boiling 0.1 M H_2SO_4 for 30 min and washed several times with ultrapure water, followed by placing in absolute ethanol overnight.

Apparatus. X-ray diffraction measurements were performed on a diffractometer (XRD-6000, Shimadzu, Japan) with Cu Kα radiation (λ = 1.5405 Å). The morphology of the products was observed by a Hitachi S4800 field-emission scanning electron microscopy (FESEM) and a JEOL JEM 200CX transmission electron microscopy (TEM, 200 kV). The Brunauer−Emmett−Teller (BET) specific surface area of the products was obtained using an automated sorption analyzer (ASA

DOI: 10.1021/acsami.6b03425
ACS Appl. Mater. Interfaces 2016, 8, 16170−16177

2020M, Micromeritics, USA). The X-ray photoelectron spectra (XPS) were taken on an electron energy spectrometer (K-alpha, Thermo Scientific, USA) using Al Kα (1486.6 eV) as the X-ray excitation source. Electrochemical impedance spectroscopy (EIS) was recorded on an Autolab PGSTAT12 (Eco chemie, BV, The Netherlands). The used amplitude was ±5 mV, and the frequency range was from 1×10^{-2} to 1×10^{5} Hz. Cyclic voltammetry analyses were performed using an electrochemical workstation (CHI660D, Chenhua, China) with a conventional three-electrode system.

Bacterial Strain. *S. oneidensis* was inoculated in Luria−Bertani (LB) broth medium and incubated aerobically in a shaking flask (150 rpm, 37 °C) until the optical density (OD_{600}) reached ~2.4. The cells for using were harvested by centrifugation (6000 rpm, 5 min) and redispersed in M9 buffer that was composed of 22 mM KH_2PO_4, 42 mM Na_2HPO_4, 85.5 mM NaCl, and 1.0 mM $MgSO_4$. The M9 buffer was sparged with N_2 to remove oxygen before using. All media were sterilized before using.

Microbial Fuel Cells Construction. Universal H-shaped two-chamber MFCs were constructed as described previously.[40] The two chambers, anodic and cathodic, were separated by a proton exchange membrane (Nafion 211, Dupont Co). The cathode was a carbon paper (2 cm × 3 cm, HeSen Electrical Corporation, Shanghai, China), which was connected to a resistance box as well as anode (graphite rod, 3D G/Fe_3O_4 foams, 3D G/MWCNTs foams, or 3D G/MWCNT/Fe_3O_4 foams electrodes) with titanium wire. The anodic chamber was filled with 100 mL of bacterial cell-cotained M9 buffer solution with 5% LB broth, and the cathode chamber contained 100 mL of phosphate buffer (100 mM, pH 7.4) and $K_3Fe(CN)_6$ (50 mM) solution. The MFCs started with adding lactate (1.5 mL) to anodic chamber, and the voltages across a 500 Ω external resistor were recorded. Additional lactate was added when the operating voltage dropped below 0.05 V. The polarization and power-density curves were obtained by varying the external resistance (9000−100 Ω) and using a multimeter to measure the cell voltage. The MFCs were operated at 25 °C with an anaerobic atmosphere.

Scanning Electron Microscopy Analysis. Electrodes with biofilm were removed from MFCs and subsequently cut into several pieces. After fixed in 2.5% glutaraldehyde for 2 h, the pieces were washed with M9 buffer solution and then dehydrated in increasing concentrations of ethanol solutions (25%, 50%, 75%, 85%, 95%, and 100%). Finally, they were dried in a vacuum oven (2 h, 40 °C). The internal and external surfaces of the dried pieces were coated with a thin layer of gold metal using an automated sputter coater (2 Kv, Emitech K550). Then, they were examined with a field emission SEM (S4800 Hitachi, Japan).

Phospholipids Analysis for Determining Microbial Biomass. Electrodes with biofilm were removed from MFCs and analyzed according to the procedure reported previously.[41−43] The absorbance at 610 nm was determined using a spectro-photometer (3600 Shimadzu, Japan). The concentrations of phosphate were calculated by using the regression line from a standard curve. The total active biomass of electrodes was obtained by using the conversion factor of 191.7 μg of biomass-C per 100 mmol of phospholipid.[44]

Bacterial Cells Viability Analysis. H-shaped two-chamber MFCs equipped with two 3D G/MWCNT/Fe_3O_4 foams were constructed. The foams were separately removed in 100 and 500 h after operation. For comparison, identical MFCs with two 3D G/MWCNT foams were constructed, and the foams were removed with the same procedure as earlier. The viability of bacteria in the foams removed from MFCs was visualized through a Nikon Ti-E inverted fluorescent microscope equipped with a high-resolution CCD camera (DS-Ri1, Nikon Corporation, Japan). The 3D electrodes were cut into small pieces (~1 mm height) using a scalpel, and the pieces were then immersed into 20 mL of phosphate buffer (10 mM, pH 7.4) containing 1 mL of calcein-AM fluorescent dyes (2 μM, Keygen Biotech Co. Ltd., Nanjing, China) for 30 min. To remove unbound residual dyes, the pieces were immersed into phosphate buffer for 10 min and repeated three times. The excitation wavelength was 490 nm, and a BP500−550 emission filter was used for green fluorescence.

RESULTS AND DISCUSSION

Characterization of 3D G/MWCNTs/Fe_3O_4 Foams. The fabrication of 3D G/MWCNTs/Fe_3O_4 foams is illustrated in Scheme 1. Graphene oxide (GO) was coupled with MWCNTs through $\pi-\pi$ stacking between aromatic rings in their carbon skeletons,[45] while Fe^{3+} cations were preassembled on the negatively charged GO surface due to the abundant surface oxygen-containing functional groups.[46] During the hydrothermal process, GO colloids were reduced and shrank into a 3D network while enwrapping MWCNTs and resultant Fe_3O_4 nanospheres in a monolithic manner. The obtained 3D G/MWCNT/Fe_3O_4 foams displayed a column-shaped macrostructure with a diameter of ~1.3 cm and a height of 0.25 cm (Figure S1). The morphology of as-synthesized 3D G/MWCNTs/Fe_3O_4 foams was investigated by FESEM and TEM. As shown in Figure 1a, interconnected networks create

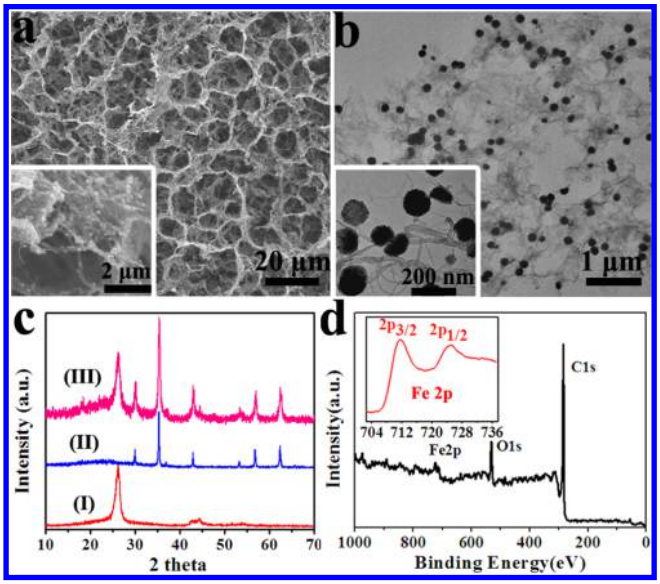

Figure 1. SEM (a) and TEM (b) images of 3D macroporous G/MWCNTs/Fe_3O_4 foams. (insets) The high-magnification images. (c) XRD patterns of MWCNTs (I), Fe_3O_4 (II), and 3D macroporous G/MWCNTs/Fe_3O_4 foams (III). (d) XPS survey spectrum of 3D macroporous G/MWCNTs/Fe_3O_4 foams, the inset corresponding to Fe 2p spectrum.

continuous macropores of ~10 μm, which can be beneficial for bacteria (~2 μm) penetration into the interior structure.[25,26,47] The magnified image shows that Fe_3O_4 nanospheres are attached on both sides of graphene sheets, while MWCNTs bridge the gaps between graphene sheets (Figure 1a inset). TEM image reveals that Fe_3O_4 nanospheres (100−150 nm) and MWCNTs are well-dispersed on graphene sheets (Figure 1b and 1b inset). Moreover, EDX analysis and elemental mapping image confirm the presence of C, O, and Fe elements in the material (Figures S2 and S3), demonstrating the successful formation of G/MWCNTs/Fe_3O_4 ternary composite foams.

The crystal structure of the as-obtained product was examined by XRD analysis (Figure 1c). The peak at 2θ = 26° is observed for MWCNTs,[48] while the peaks at 2θ = 30.3°, 35.7°, 43.3°, 54.1°, 57.4°, 62.9°, corresponding to (2 2 0), (3 1 1) (4 0 0), (4 2 2), (5 1 1), and (4 4 0) are observed for Fe_3O_4.[49] As for the 3D macroporous G/MWCNTs/Fe_3O_4 foams, all the characteristic peaks of Fe_3O_4 and MWCNTs

DOI: 10.1021/acsami.6b03425
ACS Appl. Mater. Interfaces 2016, 8, 16170−16177

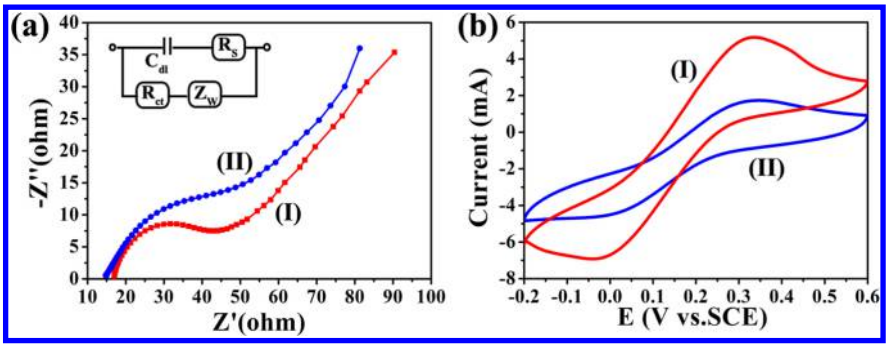

Figure 2. (a) EIS Nyquist plots of different anodes in 2 mM $[Fe(CN)_6]^{3-/4-}$ and 0.2 M KCl solution, the inset is the Randles equivalent circuit used to fit the EIS data. (b) Cyclic voltammograms of different anodes in 5.0 mM $[Fe(CN)_6]^{3-/4-}$ and 0.1 M Na_2SO_4 at a scan rate of 100 mV s^{-1}. (I) 3D G/MWCNTs/Fe_3O_4 electrode, (II) 3D G/Fe_3O_4 electrode.

are observed, demonstrating the coexistence of Fe_3O_4 and MWCNTs in the composite networks. The XPS was used to further examine the structure of as-prepared G/MWCNTs/Fe_3O_4. As shown in Figure 1d, the C 1s, O 1s, and Fe 2p bands are detected in the composite. The two peaks located at 711 and 725 eV in the magnified spectrum are attributed to the Fe $2p_{3/2}$ and Fe $2p_{1/2}$ spin orbit peaks of Fe_3O_4 (inset of Figure 1d).[50] The high-resolution C 1s spectra shows that the intensities of all peaks coming from C−OH, C−O, and C═O (285.6, 286.6, and 288.4 eV) remarkably decrease in comparison with that of GO, indicating that most of the oxygen-containing groups in GO precursor were removed during the one-pot hydrothermal process (Figure S4). In addition, Raman spectra further confirms the reduction of GO (Figure S5). Besides, the peak at 1580 cm^{-1} is designated as D band of MWCNTs,[48] implying the existence of MWCNTs in the composite.

Electrochemical Properties of 3D G/MWCNTs/Fe_3O_4 Electrode. To evaluate the contribution of MWCNTs to the ternary composite, 3D G/Fe_3O_4 foams (see the SEM images in Figure S6a,b) were prepared using a similar procedure as control. On the basis of their N_2 adsorption−desorption isotherms recorded in Figure S7a,b, the BET specific surface area of G/MWCNTs/Fe_3O_4 foams was calculated to be 168.9 m^2 g^{-1}, remarkably higher than that of G/Fe_3O_4 foams (83.1 m^2 g^{-1}), indicating that the introduction of MWCNTs is effective to inhibit the aggregation of graphene. Apart from the efficacy of spacing graphene nanosheets, MWCNTs could also serve as conductive pathways for electron transport in the electrode substrate,[29] which was verified by the decrease of charge transfer resistance (R_{ct}) from 68.9 to 27.5 Ω after the addition of MWCNTs (Figure 2a). Moreover, cyclic voltammetry (CV) suggested that the electrochemical active surface area of 3D G/MWCNTs/Fe_3O_4 anode was much larger than that of the 3D G/Fe_3O_4 electrode (Figure 2b). As a result of the morphological and electrical merits, the introduction of MWCNTs is supposed to further improve the bacteria-loading capacity of this 3D ternary electrode and enhance EET between bacteria and electrode.

Bacteria-Hosting Capability of 3D G/MWCNTs/Fe_3O_4 Electrode. To explore the value of Fe_3O_4 for the bacteria-hosting capability of 3D G/MWCNTs/Fe_3O_4 foams, 3D G/MWCNTs foams (see the SEM images in Figure S6c,d) were also prepared for comparison. After incubation with *Shewanella oneidensis* in typical H-shaped MFCs, the adhesion properties of bacterial cells on those foams were investigated. As observed under SEM (Figure 3a), a multilayered biofilm was formed on

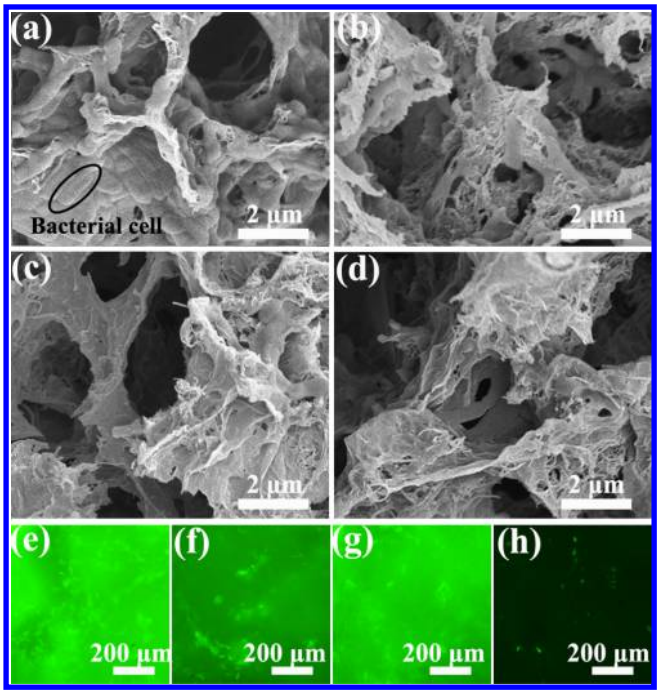

Figure 3. SEM images of *S. oneidensis* MR-1 cells on the surface (a, c) and interior (b, d) of 3D G/MWCNTs/Fe_3O_4 (a, b), and 3D G/MWCNTs foams (c, d) after 100 h of incubation in MFCs with *S. oneidensis* MR-1 cells. Inverted fluorescent microscopic images of *S. oneidensis* MR-1 cells grown in 3D G/MWCNTs/Fe_3O_4 (e, g) and 3D G/MWCNTs (f, h) foams for 100 and 500 h, respectively, after staining with calcein-AM fluorescent dye.

the surface of 3D G/MWCNTs/Fe_3O_4 foams. The SEM images of the electrode after cross-cutting display that bacterial cells also adhere to the inner macroporous architecture of the foams to form a biofilm (Figure 3b). In contrast, in the absence of Fe_3O_4, both external and internal surface of the 3D G/MWCNTs foams were coated with fewer bacterial cells, leaving large area of substrate uncovered (Figure 3c,d). The total amount of active biomass from 3D G/MWCNTs/Fe_3O_4 foams was calculated to be 21.69 mg·cm^{-3} by the phospholipids analysis, while that of 3D G/MWCNTs foams was 4.34 mg·cm^{-3}. To better understand the high bacteria-hosting capability of 3D G/MWCNTs/Fe_3O_4 anode, a comparison of porous structure between 3D G/MWCNTs and 3D G/MWCNTs/Fe_3O_4 foams was made. On the basis of N_2 adsorption−desorption analysis (Figure S7a,c), the BET specific surface areas of these two foams were approximate (168.9 m^2 g^{-1} for

DOI: 10.1021/acsami.6b03425
ACS Appl. Mater. Interfaces 2016, 8, 16170−16177

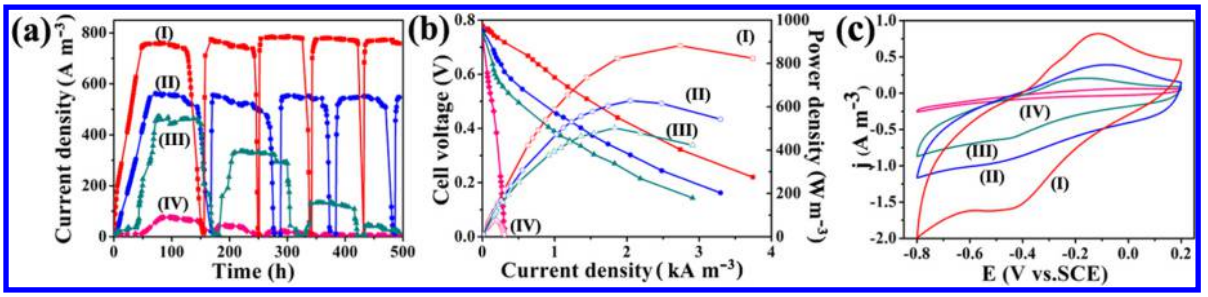

Figure 4. Constant-load discharge curve (a), and polarization and power-density curves (b) of MFCs with different electrodes. (c) CVs of different biofilm-attached anodes of MFCs in fresh mineral medium, scan rate: 10 mV s^{-1}. (I) 3D G/MWCNTs/Fe_3O_4 foams, (II) 3D G/Fe_3O_4 foams, (III) 3D G/MWCNTs foams, and (IV) graphite rod.

3D G/MWCNTs/Fe_3O_4 foams and 142.4 m^2 g^{-1} for 3D G/MWCNTs), and their pore sizes both center at 3.5 nm (Figure S8a,c). Additionally, as estimated from SEM images, the size distribution of micrometer-scale pores in 3D G/MWCNTs foams was similar to that of 3D G/MWCNTs/Fe_3O_4 foams (Figure S9a,c), which suggested that they provided analogous microchannels for bacteria penetration. Considering the similar contribution from their approximate porous structures, the superior bacteria-hosting capability of 3D G/MWCNTs/Fe_3O_4 anode can be mainly attributed to the strong chemotactic behavior of DIRB toward Fe_3O_4 caused by the high affinity between the c-type cytochromes (MtrC and OmcA) on the outer membrane of DIRB and Fe (III) oxide.[35,36,51]

Moreover, the inverted fluorescent microscope was also used to demonstrate the enhanced metabolic activity of DIRB cells on the 3D G/MWCNTs/Fe_3O_4 foams. After the MFCs operation for 100 and 500 h, the fluorescent microscopic images of bacterial cells grown in the foams were taken. Metabolically active (green) and inactive cells were distinguished using a calcein-AM fluorescent dye based on the differential permeability of cell membranes.[52] The 3D G/MWCNTs/Fe_3O_4 and G/MWCNTs foams both showed strong green fluorescence after 100 h of operation (Figure 3e,f), implying that a great deal of bacterial cells were alive. Notably, the relatively stronger green fluorescence of 3D G/MWCNTs/Fe_3O_4 foams could be attributed to the increased bacterial attachment compared to 3D G/MWCNTs foams. Interestingly, after 500 h of operation, the fluorescent microscopic image of 3D G/MWCNTs/Fe_3O_4 foams maintained a bright green background (Figure 3g), indicating the sustainable activity of immobilized bacterial cells, in comparison with the fairly weak fluorescence of 3D G/MWCNTs foams (Figure 3h), in which the majority of bacterial cells had been deactivated. In MFCs, microorganisms degrade organic matter, producing electrons that travel through a series of respirator enzymes in the bacterial cell and make energy for bacterial cell in the form of ATP.[53] The cytochromes MtrC and OmcA on the outer membrane of DIRB were reported to have a specific affinity with Fe (III) oxide.[35,36] Such intimate contact could increase the direct electron transfer between bacteria and electrode.[22,23] Because of the fast release of electrons in bacterial cell, the decomposition rate of organic matter would be accelerated. As a result, bacterial cells could obtain more energy from the decomposition of organic matter for growth and function in the same space of time. We thus concluded that Fe_3O_4 played an important role in keeping the activity of DIRB to support their long-term growth, in addition to the strong affinity toward DIRB.

Performance of Microbial Fuel Cells Configured with 3D G/MWCNTs/Fe_3O_4 Electrode. With the integration of excellent EET efficiency, high bacterial loading, and enhanced bacterial activity, the MFCs constructed with 3D G/MWCNTs/Fe_3O_4 foams are expected to achieve high performance. To verify this, the performance of MFCs equipped with the 3D ternary foams was tested. As shown in Figure 4a, the volumetric current density of 3D G/MWCNTs/Fe_3O_4 anode increased quickly in the initial 50 h, owing to the fast bacterial cells activation and colonization on anode surface (corresponding time course of the voltage output of the MFCs shows in Figure S10). Then, it kept at a plateau of 772 A·m^{-3} for 77 h, followed by a sharp drop due to the depletion of substrate. After replenishment of the substrate, the current density recovered quickly to the level of the first plateau. Even in the fifth cycle, the current density still reached a value as high as 782 A·m^{-3}, representing a good long-term stability. Compared to commonly used graphite rod, this 3D anode exhibited an 11-fold increase in biocurrent production (772 vs 67 A·m^{-3}), faster starting up (40 vs 85 h), and extremely higher stability. To further clarify the functions of each component in the real practice, the characteristics of MFCs with 3D G/MWCNTs and G/Fe_3O_4 as anodes were assessed in addition. Notably, 3D G/MWCNTs anode possessed starting time (80 h) and degradation behavior similar to graphite rod but starkly different from the ternary composite. This outcome implied that the Fe_3O_4 component took the responsibility of shortening the starting time and increasing life cycles, which should be originated from the enhanced DIRB−anode interaction and the long-term activity of DIRB. However, in the absence of MWCNTs, the maximum current density of 3D G/Fe_3O_4 anode was declined to 562 A·m^{-3}, reflecting the importance of MWCNTs on enlarging the electrochemical active surface area and facilitating EET. Moreover, the power density and polarization curves were also tested by varying the external load resistance (Figure 4b). The MFC based on the 3D G/MWCNTs/Fe_3O_4 anode produced a maximum volumetric power density of 882 W·m^{-3}, significantly higher than those of graphite rod (76 W·m^{-3}) and binary composites (502 and 628 W·m^{-3} for 3D G/MWCNTs and G/Fe_3O_4, respectively). Even compared to the previously reported high-output MFCs with 3D anode,[27,54,55] the proposed MFC with 3D G/MWCNTs/Fe_3O_4 anode possessed comparable output power density. In addition, unlike those in which the current density usually degraded from the third operation cycles, our MFC held stable current density at the high level during five operation cycles, exhibiting its unique merit over the reported 3D anode-equipped MFCs. However, compared to counterpart MFCs with stability level approximate to this work,[20,56,57] our

DOI: 10.1021/acsami.6b03425
ACS Appl. Mater. Interfaces 2016, 8, 16170−16177

proposed MFC produced 1−3 times higher current output. Taken together, this extraordinary character of long-term stability at high output manifests the application potential of this triple-component 3D anode in MFCs.

To get further insight into the influence of the 3D G/MWCNTs/Fe_3O_4 anode on biocurrent generation, the graphite rod, 3D G/MWCNTs, 3D G/Fe_3O_4, and 3D G/MWCNTs/Fe_3O_4 anodes after 100 h of incubation in MFCs were used for CV analysis. As opposed to the flat CV curve of graphite rod anode (Figure 4c, line IV), the 3D G/MWCNTs/Fe_3O_4 anode had one pair of obvious redox peaks at −0.14 and −0.46 V (vs SCE, line I), which were in good accordance with the electrochemical response of the OM c-cyts of *Shewanella*.[58,59] The result suggested that the 3D G/MWCNTs/Fe_3O_4 anode was able to harvest electrons via direct electron transfer from OM c-cyts, which was inhibited on the conventional graphite rod anode. Meanwhile, the redox peaks of binary composite anodes (3D G/Fe_3O_4, line II and G/MWCNTs, line III) respectively appeared weaker than that of 3D G/MWCNTs/Fe_3O_4 anode, further highlighting the indispensability of both MWCNTs and Fe_3O_4 components in enhancing the direct electron transfer. As reported previously, the use of CNTs could facilitate the electrode to get closer to the active center of OM c-cyts.[60] Furthermore, the modification of Fe_3O_4 has also been demonstrated to increase the kinetic activity of electrode.[61] Therefore, the introduction of MWCNTs and Fe_3O_4 could be regarded as the essential factors for enhancing direct electron transfer from OM c-cyts to 3D G/MWCNTs/Fe_3O_4 anode.

CONCLUSIONS

In summary, the novel 3D G/MWCNTs/Fe_3O_4 foams have been successfully prepared by one-pot solvothermal method and applied as an anode for MFCs. Besides the enhanced surface area provided by the 3D macroporous structure and the high conductivity of MWCNTs, this anode possesses high bacterial loading capacity and activity-retention ability due to the incorporation of DIRB-affinity Fe_3O_4, all of which significantly contributed to the improved overall performance. By coupling morphology tailoring with composition modulation, this design upgrades both the long-term stability and output performance of MFC, which brings a promising future for the development of MFC anode materials.

ASSOCIATED CONTENT

Supporting Information

The Supporting Information is available free of charge on the ACS Publications website at DOI: 10.1021/acsami.6b03425.

Supplementary characterizations of the 3D G/MWCNTs/Fe_3O_4 foams, SEM images of 3D G/MWCNTs and G/Fe_3O_4 foams, and N_2 adsorption−desorption isotherms of 3D G/MWCNT/Fe_3O_4, G/MWCNTs, and G/Fe_3O_4 foams. (PDF)

AUTHOR INFORMATION

Corresponding Authors

*E-mail: jrzhang@nju.edu.cn. (J.-R.Z.)
*E-mail: jjzhu@nju.edu.cn. (J.-J.Z.)

Notes

The authors declare no competing financial interest.

ACKNOWLEDGMENTS

We gratefully appreciate the support from National Basic Research Program of China (2011CB933502) and the National Natural Science Foundation of China (21175065, 21375059, and 21335004). The authors extend their sincere appreciation to the Deanship of Scientific Research at King Saud Univ. for its funding this prolific Research Group (PRG-1437-32).

REFERENCES

(1) Lovley, D. R. Bug Juice: Harvesting Electricity with Microorganisms. *Nat. Rev. Microbiol.* **2006**, *4* (7), 497−508.
(2) Zhao, F.; Slade, R. C. T.; Varcoe, J. R. Techniques for the Study and Development of Microbial Fuel Cells: An Electrochemical Perspective. *Chem. Soc. Rev.* **2009**, *38* (7), 1926−1939.
(3) Massazza, D.; Parra, R.; Busalmen, J. P.; Romeo, H. E. New Ceramic Electrodes Allow Reaching the Target Current Density in Bioelectrochemical Systems. *Energy Environ. Sci.* **2015**, *8* (9), 2707−2712.
(4) Li, W.-W.; Yu, H.-Q.; He, Z. Towards Sustainable Wastewater Treatment by Using Microbial Fuel Cells-Centered Technologies. *Energy Environ. Sci.* **2014**, *7* (3), 911−924.
(5) Logan, B. E. Exoelectrogenic Bacteria That Power Microbial Fuel Cells. *Nat. Rev. Microbiol.* **2009**, *7* (5), 375−381.
(6) Logan, B. E.; Hamelers, B.; Rozendal, R.; Schröder, U.; Keller, J.; Freguia, S.; Aelterman, P.; Verstraete, W.; Rabaey, K. Microbial Fuel Cells: Methodology and Technology. *Environ. Sci. Technol.* **2006**, *40* (17), 5181−5192.
(7) Baudler, A.; Schmidt, I.; Langner, M.; Greiner, A.; Schroder, U. Does It Have to Be Carbon? Metal Anodes in Microbial Fuel Cells and Related Bioelectrochemical Systems. *Energy Environ. Sci.* **2015**, *8* (7), 2048−2055.
(8) Schroder, U.; Harnisch, F.; Angenent, L. T. Microbial Electrochemistry and Technology: Terminology and Classification. *Energy Environ. Sci.* **2015**, *8* (2), 513−519.
(9) Ding, C.-m.; Lv, M.-l.; Zhu, Y.; Jiang, L.; Liu, H. Wettability-Regulated Extracellular Electron Transfer from the Living Organism of *Shewanella loihica* PV-4. *Angew. Chem., Int. Ed.* **2015**, *54* (5), 1446−1451.
(10) Borole, A. P.; Reguera, G.; Ringeisen, B.; Wang, Z.-W.; Feng, Y.; Kim, B. H. Electroactive Biofilms: Current Status and Future Research Needs. *Energy Environ. Sci.* **2011**, *4* (12), 4813−4834.
(11) Qiao, Y.; Bao, S.-J.; Li, C. M. Electrocatalysis in Microbial Fuel Cells-from Electrode Material to Direct Electrochemistry. *Energy Environ. Sci.* **2010**, *3* (5), 544−553.
(12) Liu, H.; Cheng, S.; Logan, B. E. Power Generation in Fed-Batch Microbial Fuel Cells as a Function of Ionic Strength, Temperature, and Reactor Configuration. *Environ. Sci. Technol.* **2005**, *39* (14), 5488−5493.
(13) Zhao, C.; Wang, Y.; Shi, F.; Zhang, J.; Zhu, J.-J. High Biocurrent Generation in *Shewanella*-Inoculated Microbial Fuel Cells Using Ionic Liquid Functionalized Graphene Nanosheets as an Anode. *Chem. Commun.* **2013**, *49* (59), 6668−6670.
(14) Lowy, D. A.; Tender, L. M.; Zeikus, J. G.; Park, D. H.; Lovley, D. R. Harvesting Energy from the Marine Sediment−Water Interface II: Kinetic Activity of Anode Materials. *Biosens. Bioelectron.* **2006**, *21* (11), 2058−2063.
(15) Liu, H.; Ramnarayanan, R.; Logan, B. E. Production of Electricity during Wastewater Treatment Using a Single Chamber Microbial Fuel Cell. *Environ. Sci. Technol.* **2004**, *38* (7), 2281−2285.
(16) Chaudhuri, S. K.; Lovley, D. R. Electricity Generation by Direct Oxidation of Glucose in Mediatorless Microbial Fuel Cells. *Nat. Biotechnol.* **2003**, *21* (10), 1229−1232.
(17) Chen, S.; Hou, H.; Harnisch, F.; Patil, S. A.; Carmona-Martinez, A. A.; Agarwal, S.; Zhang, Y.; Sinha-Ray, S.; Yarin, A. L.; Greiner, A.; Schroder, U. Electrospun and Solution Blown Three-Dimensional Carbon Fiber Nonwovens for Application as Electrodes in Microbial Fuel Cells. *Energy Environ. Sci.* **2011**, *4* (4), 1417−1421.

(18) Flexer, V.; Chen, J.; Donose, B. C.; Sherrell, P.; Wallace, G. G.; Keller, J. The Nanostructure of Three-Dimensional Scaffolds Enhances the Current Density of Microbial Bioelectrochemical Systems. *Energy Environ. Sci.* **2013**, *6* (4), 1291−1298.
(19) Zhao, Y.; Watanabe, K.; Nakamura, R.; Mori, S.; Liu, H.; Ishii, K.; Hashimoto, K. Three-Dimensional Conductive Nanowire Networks for Maximizing Anode Performance in Microbial Fuel Cells. *Chem. - Eur. J.* **2010**, *16* (17), 4982−4985.
(20) Erbay, C.; Yang, G.; de Figueiredo, P.; Sadr, R.; Yu, C.; Han, A. Three-dimensional Porous Carbon Nanotube Sponges for High-Performance Anodes of Microbial Fuel Cells. *J. Power Sources* **2015**, *298*, 177−183.
(21) Zou, L.; Qiao, Y.; Wu, Z.-Y.; Wu, X.-S.; Xie, J.-L.; Yu, S.-H.; Guo, J.; Li, C. M. Tailoring Unique Mesopores of Hierarchically Porous Structures for Fast Direct Electrochemistry in Microbial Fuel Cells. *Adv. Energy Mater.* **2016**, *6* (4), 1 DOI:10.1002/aenm.201501535.
(22) Wang, W.; You, S.; Gong, X.; Qi, D.; Chandran, B. K.; Bi, L.; Cui, F.; Chen, X. Bioinspired Nanosucker Array for Enhancing Bioelectricity Generation in Microbial Fuel Cells. *Adv. Mater.* **2016**, *28* (2), 270−275.
(23) Xie, X.; Criddle, C.; Cui, Y. Design and Fabrication of Bioelectrodes for Microbial Bioelectrochemical Systems. *Energy Environ. Sci.* **2015**, *8* (12), 3418−3441.
(24) Yu, M.; Han, Y.; Cheng, X.; Hu, L.; Zeng, Y.; Chen, M.; Cheng, F.; Lu, X.; Tong, Y. Holey Tungsten Oxynitride Nanowires: Novel Anodes Efficiently Integrate Microbial Chemical Energy Conversion and Electrochemical Energy Storage. *Adv. Mater.* **2015**, *27* (19), 3085−3091.
(25) Yong, Y.-C.; Dong, X.-C.; Chan-Park, M. B.; Song, H.; Chen, P. Macroporous and Monolithic Anode Based on Polyaniline Hybridized Three-Dimensional Graphene for High-Performance Microbial Fuel Cells. *ACS Nano* **2012**, *6* (3), 2394−2400.
(26) He, Z.; Liu, J.; Qiao, Y.; Li, C. M.; Tan, T. T. Y. Architecture Engineering of Hierarchically Porous Chitosan/Vacuum-Stripped Graphene Scaffold as Bioanode for High Performance Microbial Fuel Cell. *Nano Lett.* **2012**, *12* (9), 4738−4741.
(27) Xie, X.; Yu, G.; Liu, N.; Bao, Z.; Criddle, C. S.; Cui, Y. Graphene-Sponges as High-Performance Low-Cost Anodes for Microbial Fuel Cells. *Energy Environ. Sci.* **2012**, *5* (5), 6862−6866.
(28) Tung, V. C.; Chen, L.-M.; Allen, M. J.; Wassei, J. K.; Nelson, K.; Kaner, R. B.; Yang, Y. Low-Temperature Solution Processing of Graphene−Carbon Nanotube Hybrid Materials for High-Performance Transparent Conductors. *Nano Lett.* **2009**, *9* (5), 1949−1955.
(29) Fan, Z.; Yan, J.; Zhi, L.; Zhang, Q.; Wei, T.; Feng, J.; Zhang, M.; Qian, W.; Wei, F. A Three-Dimensional Carbon Nanotube/Graphene Sandwich and Its Application as Electrode in Supercapacitors. *Adv. Mater.* **2010**, *22* (33), 3723−3728.
(30) Aboutalebi, S. H.; Chidembo, A. T.; Salari, M.; Konstantinov, K.; Wexler, D.; Liu, H. K.; Dou, S. X. Comparison of GO, GO/MWCNTs Composite and MWCNTs as Potential Electrode Materials for Supercapacitors. *Energy Environ. Sci.* **2011**, *4* (5), 1855−1865.
(31) Zhou, M.; Chi, M.; Luo, J.; He, H.; Jin, T. An Overview of Electrode Materials in Microbial Fuel Cells. *J. Power Sources* **2011**, *196* (10), 4427−4435.
(32) Nakamura, R.; Kai, F.; Okamoto, A.; Newton, G. J.; Hashimoto, K. Self-Constructed Electrically Conductive Bacterial Networks. *Angew. Chem., Int. Ed.* **2009**, *48* (3), 508−511.
(33) Qian, F.; Wang, H.; Ling, Y.; Wang, G.; Thelen, M. P.; Li, Y. Photoenhanced Electrochemical Interaction between Shewanella and a Hematite Nanowire Photoanode. *Nano Lett.* **2014**, *14* (6), 3688−3693.
(34) Busalmen, J. P.; Esteve-Núñez, A.; Berná, A.; Feliu, J. M. C-Type Cytochromes Wire Electricity-Producing Bacteria to Electrodes. *Angew. Chem., Int. Ed.* **2008**, *120* (26), 4952−4955.
(35) Xiong, Y.; Shi, L.; Chen, B.; Mayer, M. U.; Lower, B. H.; Londer, Y.; Bose, S.; Hochella, M. F.; Fredrickson, J. K.; Squier, T. C. High-Affinity Binding and Direct Electron Transfer to Solid Metals by the Shewanella oneidensis MR-1 Outer Membrane c-type Cytochrome OmcA. *J. Am. Chem. Soc.* **2006**, *128* (43), 13978−13979.
(36) Lower, B. H.; Shi, L.; Yongsunthon, R.; Droubay, T. C.; McCready, D. E.; Lower, S. K. Specific Bonds between an Iron Oxide Surface and Outer Membrane Cytochromes MtrC and OmcA from *Shewanella oneidensis* MR-1. *J. Bacteriol.* **2007**, *189* (13), 4944−4952.
(37) Hummers, W. S.; Offeman, R. E. Preparation of Graphitic Oxide. *J. Am. Chem. Soc.* **1958**, *80* (6), 1339−1339.
(38) Xu, Y.; Bai, H.; Lu, G.; Li, C.; Shi, G. Flexible Graphene Films via the Filtration of Water-Soluble Noncovalent Functionalized Graphene Sheets. *J. Am. Chem. Soc.* **2008**, *130* (18), 5856−5857.
(39) Xie, X.; Ye, M.; Hu, L.; Liu, N.; McDonough, J. R.; Chen, W.; Alshareef, H. N.; Criddle, C. S.; Cui, Y. Carbon Nanotube-Coated Macroporous Sponge for Microbial Fuel Cell Electrodes. *Energy Environ. Sci.* **2012**, *5* (1), 5265−5270.
(40) Zhao, C.; Gai, P.; Liu, C.; Wang, X.; Xu, H.; Zhang, J.; Zhu, J.-J. Polyaniline Networks Grown on Graphene Nanoribbons-Coated Carbon Paper with a Synergistic Effect for High-Performance Microbial Fuel Cells. *J. Mater. Chem. A* **2013**, *1* (40), 12587−12594.
(41) Liang, P.; Wang, H.; Xia, X.; Huang, X.; Mo, Y.; Cao, X.; Fan, M. Carbon Nanotube Powders as Electrode Modifier to Enhance the Activity of Anodic Biofilm in Microbial Fuel Cells. *Biosens. Bioelectron.* **2011**, *26* (6), 3000−3004.
(42) Zhang, L.; Zhu, X.; Li, J.; Liao, Q.; Ye, D. Biofilm Formation and Electricity Generation of a Microbial Fuel Cell Started Up under Different External Resistances. *J. Power Sources* **2011**, *196* (15), 6029−6035.
(43) Aelterman, P.; Freguia, S.; Keller, J.; Verstraete, W.; Rabaey, K. The Anode Potential Regulates Bacterial Activity in Microbial Fuel Cells. *Appl. Microbiol. Biotechnol.* **2008**, *78* (3), 409−418.
(44) Findlay, R. H.; King, G. M.; Watling, L. Efficacy of Phospholipid Analysis in Determining Microbial Biomass in Sediments. *Appl. Environ. Microbiol.* **1989**, *55* (11), 2888−2893.
(45) Qiu, L.; Yang, X.; Gou, X.; Yang, W.; Ma, Z.-F.; Wallace, G. G.; Li, D. Dispersing Carbon Nanotubes with Graphene Oxide in Water and Synergistic Effects between Graphene Derivatives. *Chem. - Eur. J.* **2010**, *16* (35), 10653−10658.
(46) Li, X.; Huang, X.; Liu, D.; Wang, X.; Song, S.; Zhou, L.; Zhang, H. Synthesis of 3D Hierarchical Fe_3O_4/Graphene Composites with High Lithium Storage Capacity and for Controlled Drug Delivery. *J. Phys. Chem. C* **2011**, *115* (44), 21567−21573.
(47) Xie, X.; Hu, L.; Pasta, M.; Wells, G. F.; Kong, D.; Criddle, C. S.; Cui, Y. Three-Dimensional Carbon Nanotube−Textile Anode for High-Performance Microbial Fuel Cells. *Nano Lett.* **2011**, *11* (1), 291−296.
(48) Chen, R.; Zhao, T.; Lu, J.; Wu, F.; Li, L.; Chen, J.; Tan, G.; Ye, Y.; Amine, K. Graphene-Based Three-Dimensional Hierarchical Sandwich-type Architecture for High-Performance Li/S Batteries. *Nano Lett.* **2013**, *13* (10), 4642−4649.
(49) Park, I. H.; Christy, M.; Kim, P.; Nahm, K. S. Enhanced Electrical Contact of Microbes Using Fe_3O_4/CNT Nanocomposite Anode in Mediator-Less Microbial Fuel Cell. *Biosens. Bioelectron.* **2014**, *58*, 75−80.
(50) Chen, W.; Li, S.; Chen, C.; Yan, L. Self-Assembly and Embedding of Nanoparticles by In Situ Reduced Graphene for Preparation of a 3D Graphene/Nanoparticle Aerogel. *Adv. Mater.* **2011**, *23* (47), 5679−5683.
(51) Fredrickson, J. K.; Romine, M. F.; Beliaev, A. S.; Auchtung, J. M.; Driscoll, M. E.; Gardner, T. S.; Nealson, K. H.; Osterman, A. L.; Pinchuk, G.; Reed, J. L.; Rodionov, D. A.; Rodrigues, J. L. M.; Saffarini, D. A.; Serres, M. H.; Spormann, A. M.; Zhulin, I. B.; Tiedje, J. M. Towards Environmental Systems Biology of *Shewanella*. *Nat. Rev. Microbiol.* **2008**, *6* (8), 592−603.
(52) Katuri, K.; Ferrer, M. L.; Gutierrez, M. C.; Jimenez, R.; del Monte, F.; Leech, D. Three-Dimensional Microchanelled Electrodes in Flow-Through Configuration for Bioanode Formation and Current Generation. *Energy Environ. Sci.* **2011**, *4* (10), 4201−4210.
(53) Logan, B. E. *Microbial Fuel Cells;* John Wiley & Sons, Inc: Hoboken, NJ, 2008.

DOI: 10.1021/acsami.6b03425
ACS Appl. Mater. Interfaces 2016, 8, 16170−16177

(54) Yong, Y.-C.; Yu, Y.-Y.; Zhang, X.; Song, H. Highly Active Bidirectional Electron Transfer by a Self-Assembled Electroactive Reduced-Graphene-Oxide-Hybridized Biofilm. *Angew. Chem., Int. Ed.* **2014**, *53* (17), 4480−4483.
(55) Wang, H.; Wang, G.; Ling, Y.; Qian, F.; Song, Y.; Lu, X.; Chen, S.; Tong, Y.; Li, Y. High Power Density Microbial Fuel Cell with Flexible 3D Graphene-Nickel Foam as Anode. *Nanoscale* **2013**, *5* (21), 10283−10290.
(56) Nguyen, T.-H.; Yu, Y.-Y.; Wang, X.; Wang, J.-Y.; Song, H. A 3D Mesoporous Polysulfone-Carbon Nanotube Anode for Enhanced Bioelectricity Output in Microbial Fuel Cells. *Chem. Commun.* **2013**, *49* (91), 10754−10756.
(57) Erbay, C.; Pu, X.; Choi, W.; Choi, M.-J.; Ryu, Y.; Hou, H.; Lin, F.; de Figueiredo, P.; Yu, C.; Han, A. Control of Geometrical Properties of Carbon Nanotube Electrodes towards High-Performance Microbial Fuel Cells. *J. Power Sources* **2015**, *280*, 347−354.
(58) Deng, L.; Guo, S.; Liu, Z.; Zhou, M.; Li, D.; Liu, L.; Li, G.; Wang, E.; Dong, S. To Boost C-type Cytochrome Wire Efficiency of Electrogenic Bacteria with Fe_3O_4/Au Nanocomposites. *Chem. Commun.* **2010**, *46* (38), 7172−7174.
(59) Peng, L.; You, S.-J.; Wang, J.-Y. Carbon Nanotubes as Electrode Modifier Promoting Direct Electron Transfer from *Shewanella oneidensis*. *Biosens. Bioelectron.* **2010**, *25* (5), 1248−1251.
(60) Liu, X.-W.; Huang, Y.-X.; Sun, X.-F.; Sheng, G.-P.; Zhao, F.; Wang, S.-G.; Yu, H.-Q. Conductive Carbon Nanotube Hydrogel as a Bioanode for Enhanced Microbial Electrocatalysis. *ACS Appl. Mater. Interfaces* **2014**, *6* (11), 8158−8164.
(61) Peng, X.; Yu, H.; Wang, X.; Zhou, Q.; Zhang, S.; Geng, L.; Sun, J.; Cai, Z. Enhanced Performance and Capacitance Behavior of Anode by Rolling Fe_3O_4 into Activated Carbon in Microbial Fuel Cells. *Bioresour. Technol.* **2012**, *121*, 450−453.

DOI: 10.1021/acsami.6b03425
ACS Appl. Mater. Interfaces 2016, 8, 16170−16177